Applied Energy 215 (2018) 468–478

Contents lists available at ScienceDirect

Applied Energy

journal homepage: www.elsevier.com/locate/apenergy

Microencapsulated phase change materials with composite titania-polyurea (TiO_2-PUA) shell

Aiqin Zhao[a], Jinliang An[b], Jinglei Yang[c], En-Hua Yang[a,*]

[a] School of Civil and Environmental Engineering, Nanyang Technological University, Singapore 639798, Singapore
[b] School of Energy Science and Engineering, University of Electronic Science and Technology of China, Chengdu 611731, China
[c] Department of Mechanical and Aerospace Engineering, Hong Kong University of Science and Technology, Clear Water Bay, Hong Kong, China

HIGHLIGHTS

- A novel approach to synthesize MEPCMs with composite TiO_2-PUA shell at low temperature.
- The MEPCMs have a well-defined core–shell structure with around 73 wt.% of core fraction.
- The composite shell effectively lowers the evaporation and prevents leakage of the core material.
- The MEPCMs show mitigated supercooling, faster thermal response, and high thermal storage capacity.
- TiO_2-PUA MEPCM-modified cement pastes showed distinct latent heat storage capacity.

ARTICLE INFO

Keywords:
Latent heat storage
Phase change material (PCM)
Microencapsulation
Titanium dioxide (TiO_2)
Polyurea (PUA)
Composite shell

ABSTRACT

This paper presents a novel approach to synthesize microencapsulated phase change materials (MEPCMs) with composite titania-polyurea (TiO_2-PUA) shell at low temperature. MEPCM pre-microcapsules with PUA shell were first synthesized through interfacial polymerization in oil-in-water emulsion, followed by deposition of TiO_2 on the surface of pre-microcapsules in solution by means of the liquid phase deposition (LPD) method at low temperature. The two-step synthesis approach results in high yield of microcapsules and the MEPCMs with composite TiO_2-PUA shell integrate advantages of both organic and inorganic shells. Results show that the MEPCMs have a well-defined core–shell structure with around 73 wt.% of core fraction and dense composite TiO_2-PUA shell, which is thermally stable and durable and effectively lowers the evaporation and prevents leakage of the core material even under repeated heating and cooling. The MEPCMs also show mitigated supercooling, faster thermal response, and high thermal storage capacity. TiO_2-PUA MEPCM-modified cement pastes showed distinct latent heat storage capacity.

1. Introduction

Latent heat storage has shown great potential to enhance thermal comfort [1,2] and energy efficiency [3–7]. The main advantage of latent heat storage is the high storage density in small temperature intervals, which can be fulfilled by using phase change materials (PCMs). Studies have reported that building envelopes integrated with PCMs can potentially save 10–30% of the annual cooling and heating loads for buildings in various climate zones in the US [8,9] and even in tropical Singapore [10]. The most widely used PCMs in heat storage are those changing phase from solid to liquid. Encapsulation of PCMs is therefore necessary in many applications to hold the liquid PCM so it does not leak out into the hosting matrix [11]. Encapsulation also prevents PCM to be in contact and react with the surrounding matrix and thus avoiding changes of its composition with time [12]. Other additional benefits of encapsulation include improved compatibility of PCM with the surrounding matrix [13], reduced impact of volume change during phase transformation [14], and enhanced heat transfer to the surrounding matrix due to increased surface to volume ratio of PCM [15].

Microencapsulation is defined as encapsulation of particles with diameter smaller than 1 mm [16]. Microencapsulated PCMs (MEPCMs) are composed of the core PCM and the shell. MEPCMs with organic shell is the most common approach to encapsulate PCMs [17]. Organic shell MEPCMs have been used to fabricate thermo-regulating garment [18] and Micronal® PCM from BASF has been incorporated in building elements to enhance energy efficiency of buildings [19]. It has been

* Corresponding author.
E-mail address: ehyang@ntu.edu.sg (E.-H. Yang).

https://doi.org/10.1016/j.apenergy.2018.02.057
Received 11 October 2017; Received in revised form 15 January 2018; Accepted 8 February 2018

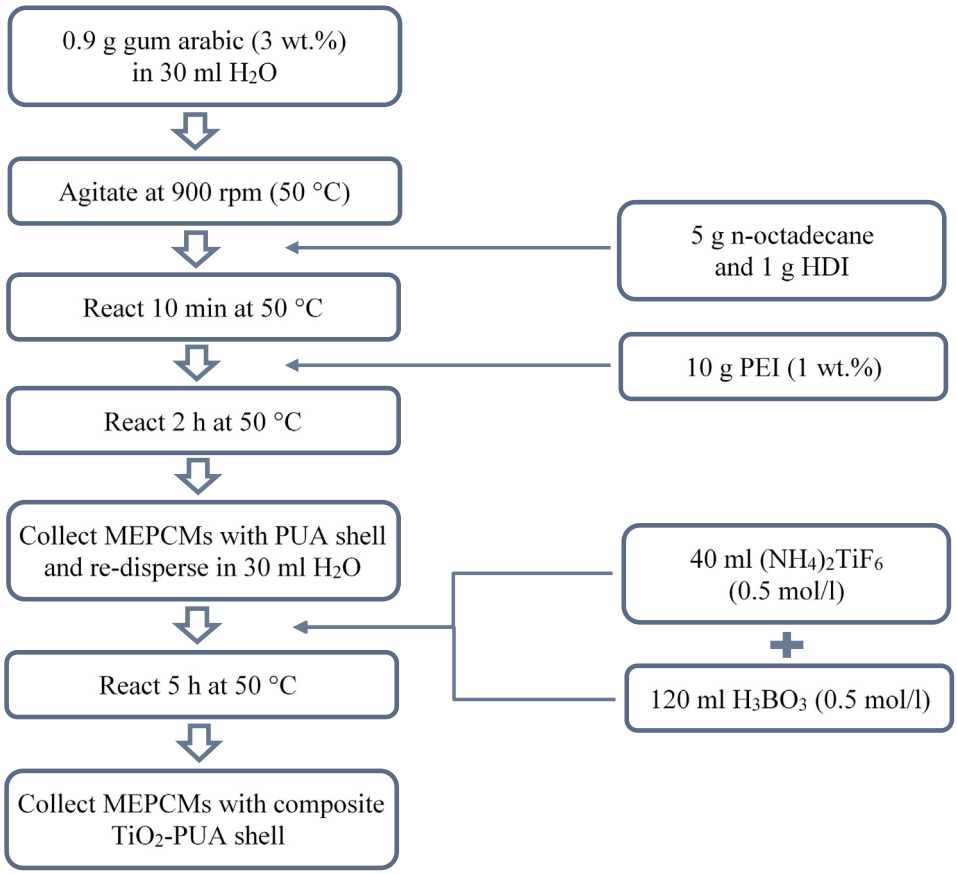

Fig. 1. Flow chart of synthesis of MEPCMs with composite TiO_2-PUA shell.

reported that MEPCM-modified skim coat possess higher heat capacity and effectively reduces envelope heat gain [20]. Despite higher toughness and good anti-leakage performance of the organic shell, utilization of organic shell MEPCMs is sometimes restricted due to their high flammability and low thermal conductivity.

These shortcomings might be overcome by encapsulating PCMs with inorganic shell [21]. Several studies have reported microencapsulation of PCM with silica (SiO_2) shell through interfacial polycondensation or sol gel synthesis [22–24]. In another work, MEPCM with calcium carbonate ($CaCO_3$) shell was fabricated [25]. However, such MEPCM is not suitable for many applications due to poor chemical stability of the $CaCO_3$ shell. Titanium dioxide (TiO_2) with several times higher thermal conductivity [26] and better mechanical properties than SiO_2 [27] can be a potential inorganic shell material for MEPCMs. In addition, it is plausible to impart photocatalysis into MEPCM through the TiO_2 shell and thus the resulting MEPCMs can be multi-functional. To the best of our knowledge, MEPCMs with TiO_2 shell is rarely studied and reported. Fang et al. [28] synthesized MEPCMs with palmitic acid as the core material and TiO_2 as the shell through the sol-gel process. The other work was reported by Chai et al. [29] where *n*-eicosane was encapsulated into a crystalline TiO_2 shell through in-situ polycondensation in the sol-gel process using titanium butoxide (TBT) as the TiO_2 precursor. In these studies, the inorganic shell was directly deposited onto the surface of organic PCM micro-droplets which stabilized by surfactant [22–29]. However, emulsions are thermodynamically unstable systems which break down over time [30]. The organic PCM micro-droplets stabilized by surfactant can easily coalesce if the synthesis conditions change, such as stirring speed and temperature. Therefore, fabrication of MEPCMs with inorganic shell using PCM micro-droplets as soft template requires strict control of experimental conditions. Moreover, while pure inorganic shells may have improved flame retardancy and thermal conductivity [31], they are brittle and the anti-leakage performance is often not satisfactory [24].

To integrate the advantages of both organic shell (i.e. toughness and anti-leakage) and inorganic shell (i.e. flame retardancy and thermal conductivity), metal films were deposited onto organic shell [32] by means of sputtering, chemical vapor deposition, and electrochemical deposition [33]. However, these methods require high temperature and/or high pressure under which organic shell microcapsules are inclined to degrade. As such, deposition of inorganic material onto organic shell under mild condition using electroless deposition is highly desired.

This study presents a novel approach to synthesize MEPCMs with composite titania-polyurea (TiO_2-PUA) shell via a two-step liquid phase deposition (LPD) at low temperature. In the first step, MEPCM pre-microcapsules with polyurea (PUA) shell is synthesized through interfacial polymerization in oil-in-water emulsion. The thin PUA shell is to stabilize and prevent coalescence of PCM micro-droplets and to serve as the hard template for deposition of TiO_2. In the second step, TiO_2 deposits on the surface of pre-microcapsules in solution by means of the LPD method at low temperature. The two-step synthesis approach shall increase the yield of microcapsules and the resulting MEPCMs with composite TiO_2-PUA shell shall integrate advantages of both organic and inorganic shells. Formation mechanisms are discussed in detail and the microcapsules are characterized by means of scanning electron microscopy (SEM), energy-dispersive X-ray (EDX) spectroscopy, infrared spectroscopy (IR), thermogravimetric analysis (TGA), and differential scanning calorimetry (DSC). Parametric studies are carried out to reveal the influence of key synthesis parameters on the core fraction and thermal stability of the MEPCMs. Thermal performance of cement paste incorporating the newly developed TiO_2-PUA MEPCMs were evaluated to demonstrate their potential applications.

2. Experiments

2.1. Chemicals

Hexamethylene diisocyanate (HDI), polyethyleneimine (PEI, Mw ~ 1300), *n*-octadecane (99%), gum arabic (99.99%), ammonium hexafluorotitanate ($(NH_4)_2TiF_6$, 99.99%), boric acid (H_3BO_3, 99.99%) were purchased from Sigma Aldrich, Singapore. All chemicals were used directly without further purification.

2.2. Synthesis of MEPCMs with composite TiO_2-PUA shell

The synthesis process of MEPCMs with composite TiO_2-PUA shell is illustrated in Fig. 1. At ambient temperature, 30 ml deionized water and 0.9 g of 3 wt.% aqueous solution of gum arabic were mixed in a 200 ml beaker. The beaker was suspended in a temperature-controlled water bath on a programmable hot plate with an external temperature probe to monitor the temperature of the solution, which was agitated at 900 rpm with a digital mixer (Caframo) driving a three-bladed propeller. The solution was covered and heated to 50 °C at a constant heating rate of 5 °C/min. Mixture of 5 g *n*-octadecane and 1 g HDI was slowly dropped into the aqueous solution to create emulsion with the stirring speed at 900 rpm for 10 min. It is followed by addition of 10 g of 1 wt.% aqueous solution of PEI. After 2 h continuous agitation, the resulting MEPCMs with PUA shell (pre-microcapsules) were collected and washed with distilled water three times. After which, the pre-microcapsules were re-dispersed into 30 ml deionized water in a 200 ml beaker. Subsequently, 40 ml $(NH_4)_2TiF_6$ solution (0.5 mol/l) and 120 ml H_3BO_3 solution (0.5 mol/l) were added into the suspension solution of pre-microcapsules and reacted for 5 h at 50 °C. The resulting MEPCMs with composite TiO_2-PUA shell were collected and washed with distilled water three times and air dried at ambient condition (27 ± 3 °C and 60 ± 5%RH) for 24 h before further analysis. At the end, 5.6 g dried MEPCMs can be obtained.

2.3. Characterization

Morphology and chemical compositions of microcapsules were studied by means of a field-emission scanning electron microscope (FE-SEM, JOEL JSM-7600F) coupled with an energy-dispersive X-ray (EDX) spectrometer. MEPCMs were spread on the SEM holder and few microcapsules were broken by a razor blade. The samples were sputter-coated with a thin layer of platinum. High-resolution SEM micrographs were obtained in high vacuum mode at an appropriate acceleration. Infrared spectra of the *n*-octadecane (core material), TiO_2-PUA shell, and MEPCMs with TiO_2-PUA shell were collected from an attenuated total reflectance-Fourier transform infrared spectrometer (ATR-FTIR, Nicolet iS50) at a scanning number of 32. The pure TiO_2-PUA shell was obtained by first crushing and grinding the microcapsules, followed by washing using hexane for 3 times to remove core *n*-octadecane. The resulting shell powder was dried in ambient condition (27 ± 3 °C and 60 ± 5%RH) before further characterization.

n-octadecane, TiO_2-PUA shell, and MEPCMs with TiO_2-PUA shell were characterized by thermogravimetric analysis (TGA, TA Q500). 10 mg of samples was placed in a platinum pan and heated from room temperature to 800 °C at a constant heating rate of 10 °C/min under nitrogen purge with a flow rate of 50 ml/min. The core fraction, L_{TGA}, describes the loading content of the core material (*n*-octadecane) in microcapsules and can be estimated from the TGA result by taking the weight ratio of core material to the microcapsule through the following equation [29].

$$L_{TGA} = \frac{W_{core}}{W_{MEPCM}} \times 100\% \quad (1)$$

where W_{core} in mg is the weight of core material and W_{MEPCM} in mg is the weight of MEPCM samples. To evaluate the permeability of the microcapsules, weight loss of MEPCMs with TiO_2-PUA shell subject to an isothermal condition at 80 °C for 60 min under nitrogen atmosphere was monitored by TGA. Isothermal test on *n*-octadecane was also carried out as the control.

Thermal properties of *n*-octadecane, TiO_2-PUA shell, and MEPCMs with TiO_2-PUA shell were evaluated by means of differential scanning calorimetry (DSC, TA Q100). 5 mg of samples was enclosed in a standard aluminum pan (40 μl) and was subjected to a heating and cooling cycle from −5 to 60 °C at a constant heating (and cooling) rate of 5 °C/min with dry nitrogen as purge gas. In another test, MEPCMs with TiO_2-PUA shell was subjected to 100 cycles of heating and cooling in DSC to evaluate their durability. Encapsulation efficiency, E_{en}, which describes effective encapsulation of core material in the microcapsules [21], can be evaluated from the DSC results by taking the ratio of fusion enthalpy of microcapsules to that of *n*-octadecane as follows [34].

$$E_{en} = \frac{\Delta H_{m,MEPCM}}{\Delta H_{m,octa}} \times 100\% \quad (2)$$

where $\Delta H_{m,MEPCM}$ in J/g is the melting enthalpy of MEPCM and $\Delta H_{m,octa}$ in J/g is the melting enthalpy of bulk *n*-octadecane. Energy storage efficiency, E_{es}, which evaluates the latent heat storage efficiency of MEPCM, can be calculated from the DSC results as follows [35].

$$E_{es} = \frac{\Delta H_{m,MEPCM} + \Delta H_{c,MEPCM}}{\Delta H_{m,octa} + \Delta H_{c,octa}} \times 100\% \quad (3)$$

where $\Delta H_{c,MEPCM}$ in J/g is the freezing enthalpy of MEPCM and $\Delta H_{c,octa}$ in J/g is the freezing enthalpy of bulk *n*-octadecane. Thermal storage capability of MEPCM, C_{es}, can be determined from the DSC curves as follows [22].

$$C_{es} = \frac{E_{es}}{E_{en}} \times 100\% \quad (4)$$

2.4. Application

To demonstrate potential application of the current study, thermal performance of cement paste incorporating the newly developed TiO_2-PUA MEPCMs were explored. TiO_2-PUA MEPCMs (5 and 10 wt.% of cement content) were mixed into fresh cement pastes to prepare the samples. Pure cement paste without the addition of MEPCMs was also prepared as the control. Heat capacity of hardened specimens were determined by means of DSC.

3. Results and discussion

3.1. Formation mechanism of MEPCMs with composite TiO_2-PUA shell

Fig. 2a–c present the conceptual drawings illustrating the formation of MEPCMs with composite TiO_2-PUA shell. The synthesis starts with creating an emulsion where PCM micro-droplets (Fig. 2a) are dispersed uniformly in water. During the 10 min of emulsification, the *n*-octadecane droplets are formed and stabilized with the presence of gum arabic, a complex mixture of glycoproteins and polysaccharides. Glycoprotein is a kind of protein containing amino functional groups that is reactive to isocyanates [36]. Thus, a thin shell is partially formed from the reaction between gum arabic and HDI. Furthermore, HDI molecules (mixed with *n*-octadecane) diffuse gradually to the surface of micro-droplets and react with water to form polymer due to high reactivity of HDI. The addition of diluted PEI solution after emulsification enables the formation of PUA shell (Fig. 2b) due to the reaction between PEI and NCO groups of HDI [37]. In summary, a combination of PUA with different crosslink density in the shell wall was formed from the reaction between HDI and PEI together with secondary reactions between NCO groups of HDI or intermediate polyisocyanates and hydroxyl groups of gum arabic or water [38]. The PUA shell is thin (few μm) and MEPCM pre-microcapsules with PUA shell cannot withstand the

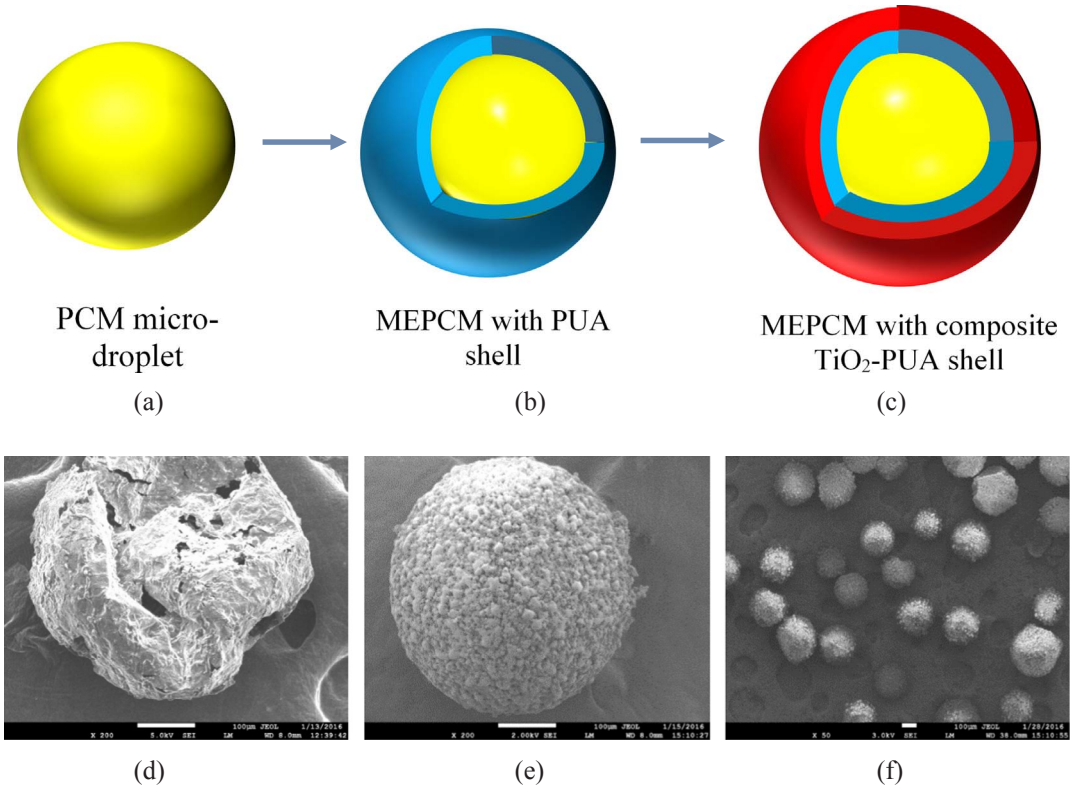

Fig. 2. Schematic drawing of (a) PCM micro-droplet, (b) MEPCMs with PUA shell, and (c) MEPCMs with TiO_2-PUA shell. Micrographs of (d) individual MEPCM with PUA shell and (e) individual MEPCM with TiO_2-PUA shell (f) Fabricated free-flowing MEPCMs.

vacuum condition and high energy beam of electrons under SEM observation as shown in Fig. 2d.

TiO_2 then deposits on the surface of pre-microcapsules (Fig. 2c). The NH_2 and NHR groups on PUA are inclined to attract TiF_6^{2-} [39]. Thus, deposition of TiO_2 on the PUA shell occurs naturally as shown in Eqs. (5) and (6) [40,41].

$$[TiF_6]^{2-} + n\ H_2O \rightleftharpoons [TiF_{6-n}(OH)_n]^{2-} + n\ HF \quad (5)$$

$$[Ti(OH)_6]^{2-} + 2H^+ \rightleftharpoons TiO_2 + 4H_2O \quad (6)$$

$$H_3BO_3 + 4HF \rightleftharpoons HBF_4 + 3H_2O \quad (7)$$

Hydrolysis of $(NH_4)_2TiF_6$ leads to formation of TiO_2 and HF (Eqs. (5) and (6)). H_3BO_3 then reacts with HF and forms more stable HBF_4 complex (Eq. (7)) [42], which promotes further hydrolysis of $(NH_4)_2TiF_6$ and deposition of TiO_2 on the PUA shell (Eqs. (5) and (6)). With continuous reaction, the TiO_2 layer grows thicker and form a solid structure [40] on the sphere PUA template (Fig. 2d and e). The thin PUA shell effectively stabilizes and prevents coalescence of PCM micro-droplets and serves as the hard template for deposition of TiO_2. The resulting MEPCMs with TiO_2-PUA shell can be successfully collected from the solution and dried in the ambient condition (30 ± 3 °C and 60 ± 5%RH). The dried MEPCMs are free-flowing powder and white in color, as shown in Fig. 2f.

3.2. Characterization of MEPCMs with composite TiO_2-PUA shell

The resultant MEPCMs with TiO_2-PUA shell is in spherical shape (Fig. 2e) with diameter of about 300 ± 100 μm on average. Well-defined core-shell structure with a very dense shell of about 10 μm in thickness without any defects can be observed in Fig. 3a. The outer surface of the capsule presents coarsely which may be ascribed to random deposition of TiO_2 precursor and thus forming rough surface with protruding nubs-like morphology (Fig. 3b). Fig. 3c presents the EDX spectra probed from the surface of the microcapsules. The inset table in Fig. 3c reveals high quantity of titanium elements suggesting successful deposition of TiO_2 as the shell material. The thin inner PUA shell; however, is smooth (Fig. 3a), which provides a skeleton for the TiO_2 nanoparticles to assemble tightly and to form a densely sealed hard shell. The composite TiO_2-PUA shell integrates the advantages of organic material (PUA) and inorganic material (TiO_2).

Fig. 4 shows the FTIR spectra of *n*-octadecane, TiO_2-PUA shell and MEPCMs with TiO_2-PUA shell. For *n*-octadecane, the absorption at 2924 cm^{-1} and 2854 cm^{-1} are ascribed to the stretching of the alkyl C—H bond of methylene group, while the absorption peak at 1465 cm^{-1} belongs to the methylene deformation vibration [25]. For the TiO_2-PUA shell, the wide absorption peak between 3700 and 2900 cm^{-1} and center at 3332 cm^{-1} is attributed to the stretching vibration of O—H bond which chemically bound to the TiO_2 surface or belong to the water absorbed onto the TiO_2 shell [43]. IR absorption band is strong at wavenumber below 1000 cm^{-1} due to the vibrational modes of Ti—O—Ti group [44,45]. The absorption peaks at 1585 cm^{-1} and 1625 cm^{-1} are ascribed to the formation of amide bond in the PUA [46]. Specifically, the 1625 cm^{-1} band is due to the hydrogen bond between one urea carbonyl group and two N—H groups [47], which form a ring. In this ring, two PUA molecules are connected by the bidentate hydrogen bonding (CO-NH_2 amide I, 1625 cm^{-1}) through the active hydrogen atoms of the two urea donor groups (—NH—) in one urea molecule and an acceptor oxygen of the carbonyl group (—CO—) in another urea molecule. The peak at 1585 cm^{-1} indicates existence of amide II (CO-NH) and hydrogen bond [48]. As can be seen, the FTIR spectrum of MEPCMs is the superposition of the *n*-octadecane and the TiO_2-PUA shell spectra. No new peak is observed in the MEPCM spectrum which indicates no chemical interaction between the core *n*-octadecane and the TiO_2-PUA shell during the synthesis of MEPCMs.

Fig. 5a compares the TGA curves of *n*-octadecane, TiO_2-PUA shell, and MEPCMs with TiO_2-PUA shell. It shows that bulk *n*-octadecane starts to decompose at 136 °C and completely decomposes at around 187 °C. For the TiO_2-PUA shell, 24.3% of mass loss in total can be

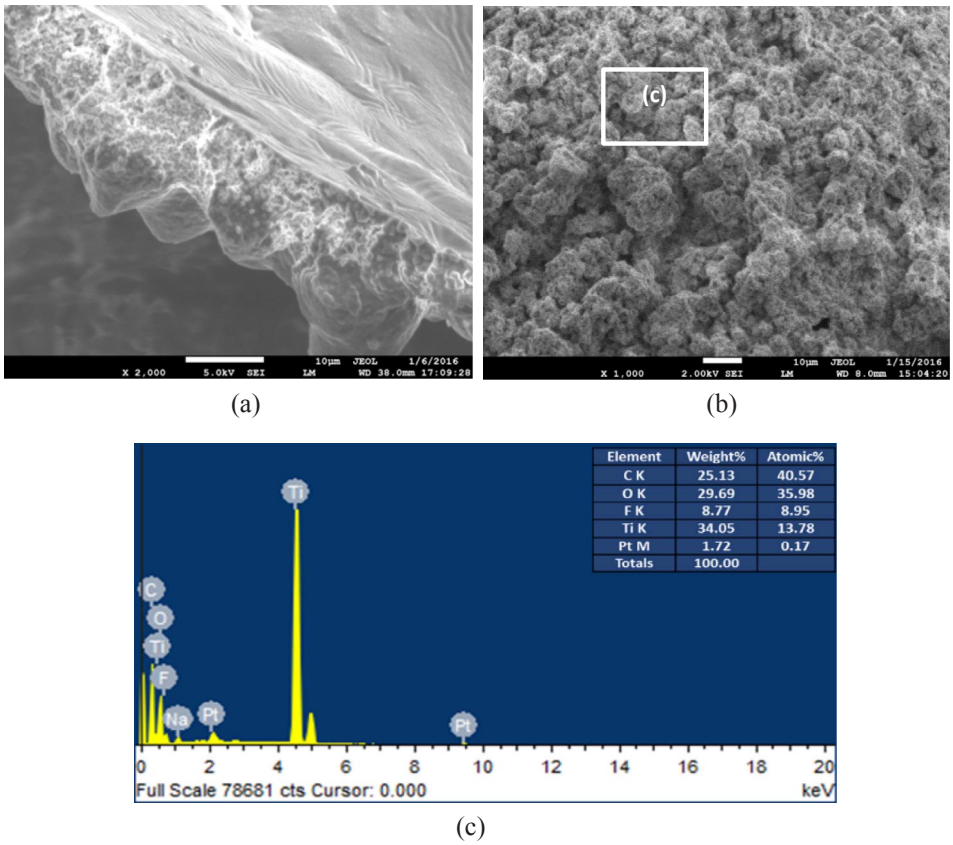

Fig. 3. Micrographs showing (a) the core-shell structure, and (b) morphology of outer surface of MEPCMs with composite TiO_2-PUA shell. (c) EDX spectrum of the outer surface of TiO_2-PUA shell.

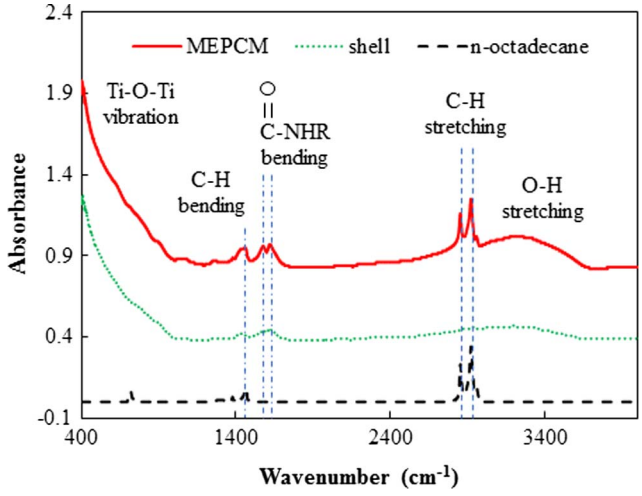

Fig. 4. FTIR spectra of *n*-octadecane, TiO_2-PUA shell, and MEPCMs with composite TiO_2-PUA shell.

observed. Except the mass loss below 105 °C which can be assigned to the H_2O evaporation, the mass loss above 250 °C is mainly ascribed to decomposition of PUA [49]. As for the MEPCMs, the decomposition of core *n*-octadecane commences at 158 °C. At around 202.3 °C, 72.83% of mass loss can be observed due to the evaporation and decomposition of core *n*-octadecane. It is noteworthy that decomposition of core *n*-octadecane in the MEPCMs is delayed by 22 and 15 °C for the starting and ending temperatures, respectively, as compared to that of bulk *n*-octadecane. This is mainly attributed to the protection from the TiO_2-PUA shell. At around 300 °C, another 5.52% mass loss is registered, which is attributed to the decomposition of PUA membrane. Overall, 21.6% mass remains after heating to 800 °C, which is ascribed to the mass of TiO_2 shell.

Fig. 5b plots the isothermal TGA curves of bulk *n*-octadecane and MEPCMs with composite TiO_2-PUA shell. It is exhibited that mass loss of bulk *n*-octadecane through volatility and evaporation is approximate 24% by weight after 1 h isothermal heating at 80 °C, while mass loss of MEPCMs is greatly reduced to be only around 3.5 wt.%. This indicates encapsulation significantly lower the evaporation of core *n*-octadecane due to the dense TiO_2-PUA shell, which effectively prevents leakage of the core material.

Fig. 6 shows the DSC thermograms of *n*-octadecane, TiO_2-PUA shell, and MEPCMs with TiO_2-PUA shell. As can be seen, TiO_2-PUA shell does not possess any latent heat storage capacity in the temperature range between −5 and 60 °C. Both bulk *n*-octadecane and MEPCMs exhibit phase change behavior. However, the area under the DSC curve of MEPCMs is smaller than that of bulk *n*-octadecane, indicating MEPCMs have less latent heat storage per unit weight of sample. This is because the TiO_2-PUA shell does not store latent heat in the current temperature range. Furthermore, the DSC curve of MEPCMs is narrower and sharper than that of bulk *n*-octadecane. This suggests that MEPCMs with composite TiO_2-PUA shell possess faster thermal response, which is an indispensable characteristic of PCM for latent heat storage and temperature modulation. The enhanced thermal response may be attributed to the large surface area of MEPCMs together with the high thermal conductivity of TiO_2 [29].

Table 1 summarizes the phase change performance and thermal characteristics of bulk *n*-octadecane, TiO_2-PUA shell, and MEPCMs with TiO_2-PUA shell. Firstly, it is obvious that the gap between the peak melting temperature T_m and the peak crystallization temperature T_c of the MEPCMs (5.3 °C) is about 3 °C less than that of bulk *n*-octadecane (8.2 °C). This implies that supercooling may be mitigated by micro-encapsulation with composite TiO_2-PUA shell. Around 72.8% by weight

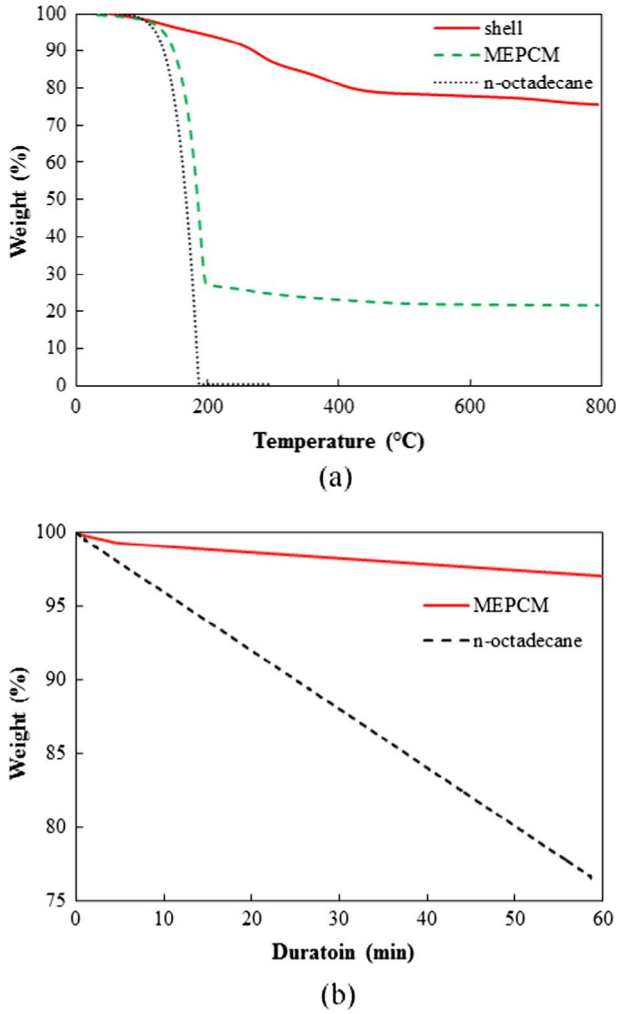

Fig. 5. (a) TGA curves of *n*-octadecane, TiO_2-PUA shell, and MEPCMs with composite TiO_2-PUA shell. (b) Isothermal TGA curves of *n*-octadecane and MEPCMs with composite TiO_2-PUA shell at 80 °C for 60 min in N_2 atmosphere.

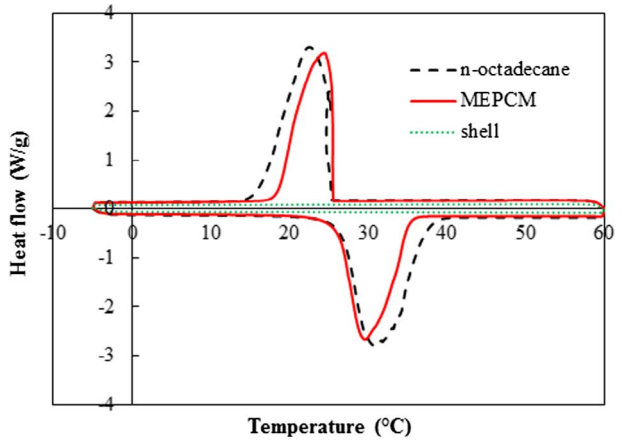

Fig. 6. DSC thermograms of *n*-octadecane, TiO_2-PUA shell, and MEPCMs with TiO_2-PUA shell.

of microcapsules is core *n*-octadecane according to the TGA result, L_{TGA}. The encapsulation ratio E_{en} based on the DSC results, which represents the latent heat storage capacity of the microcapsule, is around 77.1% that of the bulk *n*-octadecane. The encapsulation efficiency (E_{es}, 77.3%) is very close to the encapsulation ratio and thus the thermal storage capacity C_{es} of the MEPCMs can reach 99.9%, which indicates that core *n*-octadecane performs well and is able to fully exert its function during the melting and freezing cycle.

Fig. 7 shows the DSC thermogram of MEPCMs with TiO_2-PUA shell subject to 100 heating-cooling cycles. As can be seen, the peak melting/solidifying temperatures of MEPCMs at the 100th cycle (30.43/24.29 °C) remains similar to that at the 1st cycle (30.94/23.65 °C). The melting/solidifying enthalpies of the 100th cycle (165.4/165.1 J/g) is only 0.36% different from that of the 1st cycle (165.3/164.5 J/g). This shows the MEPCMs with composite TiO_2-PUA shell exhibits outstanding thermal stability and durability with nearly the same phase change temperatures and stable phase change enthalpies during repeating heating-cooling cycles.

Table 2 summarizes the yield of MEPCMs in this study. As can be seen, a total of 5.6 g dried MEPCMs can be obtained after each time of synthesis (Fig. 1) which represents 76.7% conversion rate of reactant (Table 1). 0.1 g PEI was calculated based on the addition of 10 g of 1 wt.% aqueous solution of PEI. 1.6 g TiO_2 was derived from the addition of 40 ml of 0.5 mol/l $(NH_4)_2TiF_6$ solution and molar mass of TiO_2 was taken as 80 g/mol. Furthermore, 4.0 g *n*-octadecane was successfully encapsulated (based on the 72.8% encapsulation ratio obtained from the DSC result, Table 1) which corresponds to an 80% yield of PCM. Around 60% of shell precursors (HDI, PEI, and TiO_2) was converted into the compositeTiO_2-PUA shell. The two-step synthesis approach results in high yield of microcapsules and high conversion rate of shell reactant. This is attributed to that the thin PUA shell effectively stabilizes and prevents coalescence of PCM micro-droplets and serves as the hard template for deposition of TiO_2. The NH_2 and NHR groups on PUA provide strong electrostatic attraction and promote TiO_2 deposition [39].

3.3. Parametric study

Six key synthesis parameters, including stirring speed during emulsification (900–1500 rpm), gum arabic dosage (0.6–0.9 g), $(NH_4)_2TiF_6$ dosage (2–6 g), reaction temperature for TiO_2 deposition (50–90 °C), H_3BO_3-to-$(NH_4)_2TiF_6$ ratio (1–3), and reaction duration for TiO_2 deposition (2–4 h), were studied to reveal their influence on the core fraction, thermal stability, and energy storage capacity and efficiency of the resulting MEPCMs with TiO_2-PUA shell. Reference synthesis conditions were stirring speed of 1500 rpm, gum arabic dosage of 0.9 g, $(NH_4)_2TiF_6$ dosage of 4 g, reaction temperature for TiO_2 deposition at 90 °C, H_3BO_3-to-$(NH_4)_2TiF_6$ ratio of 3, reaction duration for TiO_2 deposition of 4 h. Only one factor was changed at a time and all other factors remain unchanged as the control synthesis conditions.

3.3.1. Stirring speed during emulsification

As shown in Fig. 8a, the core fraction decreases while the isothermal weight loss increases with increasing stirring speed during the emulsion process, which is an important factor controlling the size of *n*-octadecane droplet. It has been reported that the size of PCM droplets in water emulsion decreases with increasing stirring speed [50]. In the current study, the size of pre-microcapsule reduces from 300 to 100 μm when the stirring speed increases from 900 to 1500 rpm (Table 3). Smaller droplets introduce more surface area for PUA formation and TiO_2 deposition. Both increase the shell fraction and thus core fraction decreases with reducing droplet size and increasing stirring speed. As can be seen, the core *n*-octadecane increases from 56.5 to 72.8 wt.% as the capsule size increases from 100 to 300 μm (Table 3). The latent heat storage capacity of the MEPCMs also increases from 53.9 to 77.1% with increasing size. Furthermore, microcapsules with different sizes show high C_{es} above 99%, which suggests the all MEPCMs exert their function during the melting and freezing cycle. Increase of isothermal weight loss may be attributed to the reduction of thickness, density, and/or permeability of the TiO_2-PUA shell, because the surface area of droplets increases while the same amount of precursors was used.

Fig. 9 compares the DSC curves of the MEPCMs with TiO_2-PUA shell

Table 1
Phase change performance and thermal characteristics of bulk *n*-octadecane, TiO_2-PUA shell, and MEPCMs with TiO_2-PUA shell.

Sample	Crystallization		Melting		L_{TGA} (%)	E_{en} (%)	E_{es} (%)	C_{es} (%)
	T_c (°C)	ΔH_c (J/g)	T_m (°C)	ΔH_m (J/g)				
n-octadecane	22.57	233.5 ± 0.03	30.78	235.3 ± 0.07	–	–	–	–
Shell	–	–	–	–	–	–	–	–
MEPCMs	24.36	179.8 ± 0.01	29.66	181.1 ± 0.05	72.8	77.3	77.1	99.9

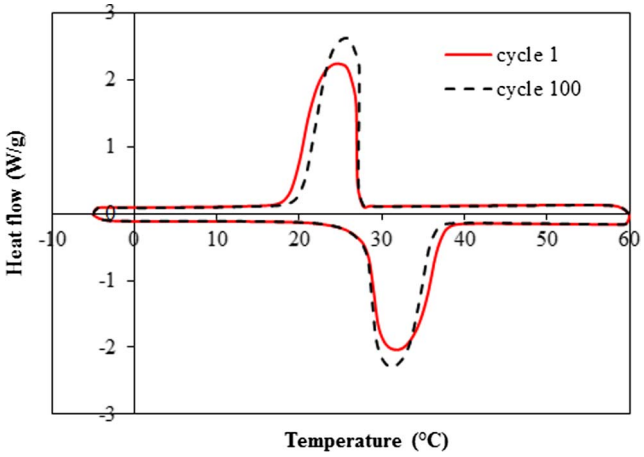

Fig. 7. DSC thermogram of MEPCMs with composite TiO_2-PUA shell subject to 100 heating-cooling cycles.

Table 2
Yield of MEPCMs with composite TiO_2-PUA shell.

	Total (g)	Core (g)	Shell (g)		
		n-octadecane	HDI	PEI	TiO_2
Reactant	7.7	5.0	1.0	0.1*	1.6#
MEPCMs	5.6	4.0^	1.6&		
Yield/conversion rate (%)	72.7	80.0	59.3		

* 0.1 g PEI was calculated based on the addition of 10 g of 1 wt.% aqueous solution of PEI.

1.6 g TiO_2 was derived from the addition of 40 ml of 0.5 mol/l $(NH_4)_2TiF_6$ solution and molar mass of TiO_2 was taken as 80 g/mol.

^ 4.0 g of core *n*-octadecane in MEPCMs was determined based on the 72.8% encapsulation ratio obtained from the DSC result (Table 1).

& 1.6 g of composite TiO_2-PUA shell in the resulting MEPCMs microcapsules.

with different sizes. As can be seen, both T_m and T_c reduce with reducing capsule size (Table 3) which has also been observed in MEPCM with different type of shell material [29]. This is because the core *n*-octadecane is confined in a micro scale space which limits the motion of *n*-octadecane molecules during phase transformation [51]. As a result, crystal defects are possibly generated in *n*-octadecane which leads to decrease in crystallization and melting temperatures [52]. Reduced microcapsule size may exacerbate such confinement effect and thus T_m and T_c reduce with reducing capsule size.

3.3.2. Gum arabic dosage

Gum arabic is the surfactant to emulsify and to stabilize the oil droplet in the emulsification. As can be seen, the core fraction decreases while the isothermal weight loss increases with increasing dosage of gum arabic (Fig. 8b). This is mainly attributed to that the amount of gum arabic has significant influence on the size of droplets [53,54]. Gum arabic reduces the interfacial tension and prevents coalescence of droplets and thus higher dosage of gum arabic results in smaller droplets, which introduces more surface area. Therefore, the core fraction of microcapsules reduces and isothermal weight loss increases due to the same reason discussed above.

3.3.3. $(NH_4)_2TiF_6$ dosage

$(NH_4)_2TiF_6$ is the precursor for deposition of TiO_2 on the surface of pre-microcapsules. As can be seen, both the core fraction and the isothermal weight loss decrease with increasing $(NH_4)_2TiF_6$ dosage (Fig. 8c). This is attributed to more TiO_2 deposits on the surface of pre-microcapsules to form a thicker, denser, and/or less permeable shell at higher $(NH_4)_2TiF_6$ dosage. This reduces the core fraction and isothermal weight loss (i.e. less leakage) of the resulting MEPCMs. Reduced leakage mitigates agglomeration of capsules and improves the free-flowing property of the dry microcapsules as shown in the inset of Fig. 8c.

3.3.4. Reaction temperature for TiO_2 deposition

Both the core fraction and the isothermal weight loss decrease with increasing reaction temperature for TiO_2 deposition (Fig. 8d). This is because more TiO_2 deposits on the pre-microcapsules at higher reaction temperature. TiO_2 deposition is a process of heterogeneous crystal nuclei formation and homogeneous growing as shown in Eqs. (5) and (6). At higher reaction temperature, the reaction equilibrium shifts towards the right-hand side of the equation, so that more TiO_2 forms and deposits on the pre-microcapsules. As a result, both the core fraction and isothermal weight loss of the resulting MEPCMs reduce. Fig. 10 shows the DSC curves of MEPCM synthesized at different temperature and Table 4 summarizes the phase change performance and thermal characteristics of the resulting MEPCMs. As can be seen, core fraction, encapsulation efficiency, and energy storage efficiency decrease with increasing reaction temperature due to less PCM per unit weight of microcapsule. However, thermal storage capacity of MEPCMs synthesized at different temperature remains similarly above 99.5%.

3.3.5. H_3BO_3-to-$(NH_4)_2TiF_6$ ratio

It can be observed that the core fraction decreases while the isothermal weight loss remains largely the same with increasing H_3BO_3-to-$(NH_4)_2TiF_6$ ratio. H_3BO_3 is the scavenger for HF (Eq. (6)) produced during hydrolysis of $(NH_4)_2TiF_6$, the precursor for TiO_2 (Eq. (5)). Higher ratio of H_3BO_3 to $(NH_4)_2TiF_6$ consumes more HF, promotes hydrolysis of $(NH_4)_2TiF_6$, and thus more TiO_2 forms during the same reaction duration [38]. As a result, more TiO_2 can deposit on the surface of pre-microcapsules to form a thicker, denser, and/or less permeable shell, which reduces the core fraction and isothermal weight loss (i.e. less leakage) and enhances the free-flowing properties (Fig. 8e inset) of the resulting MEPCMs. Fig. 11 shows the DSC curves of MEPCM synthesized at different temperature and Table 5 summarizes the phase change performance and thermal characteristics of the resulting MEPCMs. As can be seen, core fraction, encapsulation efficiency, and energy storage efficiency decrease with increasing H_3BO_3-to-$(NH_4)_2TiF_6$ ratio due to higher TiO_2 shell percentage and thus less PCM per unit weight of microcapsule. However, thermal storage capacity of MEPCMs synthesized with different H_3BO_3-to-$(NH_4)_2TiF_6$ ratio remains high (> 99%).

3.3.6. Reaction duration for TiO_2 deposition

Both the core fraction and the isothermal weight loss decrease with increasing reaction duration for TiO_2 (Fig. 8f). Extended reaction

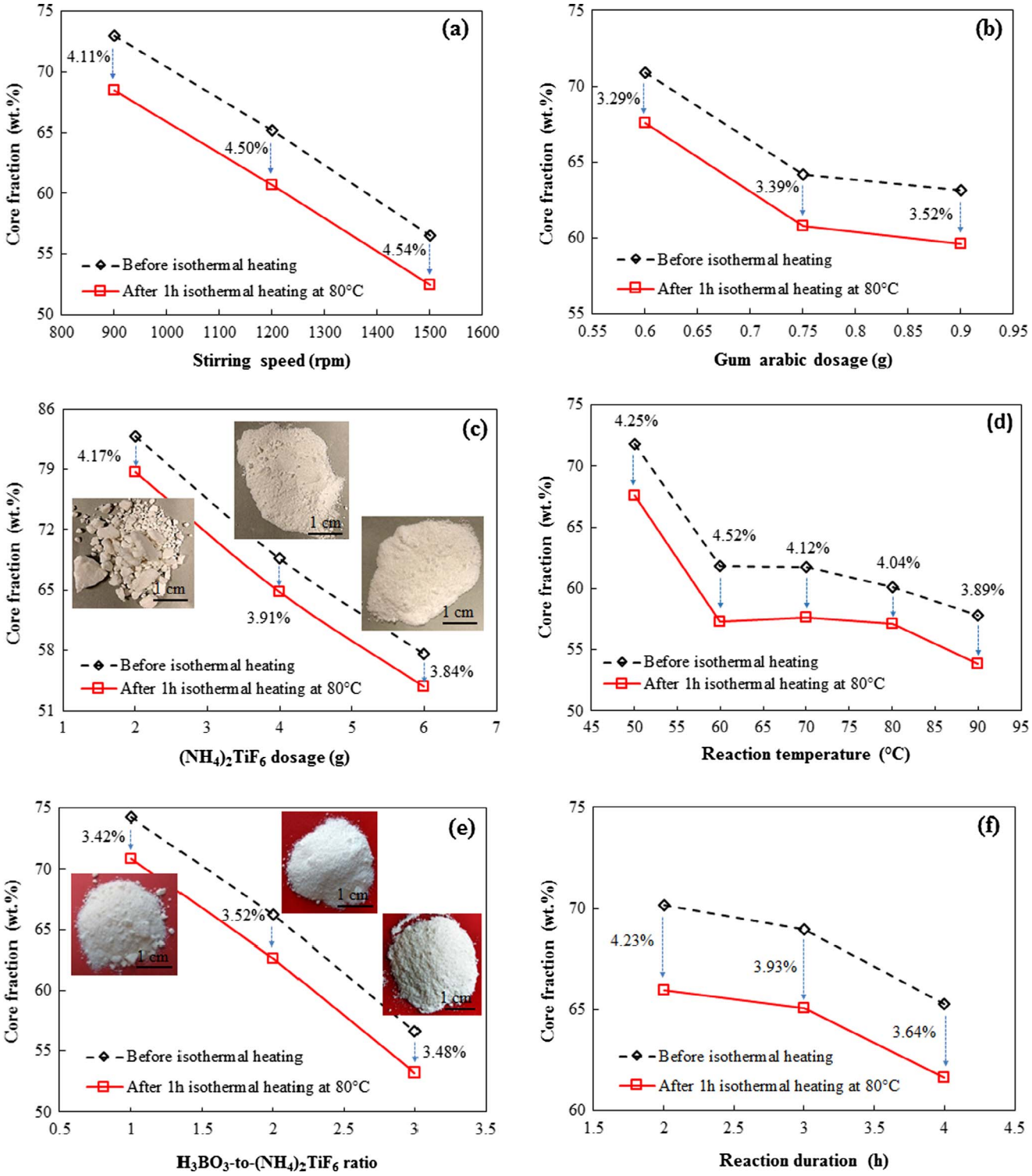

Fig. 8. Core fraction and thermal stability of MEPCMs with TiO_2-PUA shell as a function of (a) stirring speed during emulsification, (b) gum arabic dosage, (c) $(NH_4)_2TiF_6$ dosage, (d) reaction temperature for TiO_2 deposition, (e) H_3BO_3-to-$(NH_4)_2TiF_6$ ratio, and (f) reaction duration for TiO_2 deposition.

duration allows more TiO_2 to deposit onto the pre-microcapsules and to form a thicker, denser, and/or less permeable shell. This again reduces the core fraction and isothermal weight loss of the resulting MEPCMs with composite TiO_2-PUA shell.

3.4. Heat capacity of TiO_2-PUA MEPCM-modified cement paste

Fig. 12 compares the DSC curves of MEPCM-modified cement paste against the control specimen. As can be seen, pure cement paste does not possess any latent heat capacity. In contrast, TiO_2-PUA MEPCM-modified cement pastes show distinct melting and solidifying behavior. With the increase of MEPCM dosage from 0%, 5%, to 10%, the amplitude of melting/solidifying peak increases which suggests the energy storage capacity enhances with the amount of MEPCM dosage. This shows that the addition of the newly developed TiO_2-PUA MEPCMs is able to impart the energy storage capability into cement paste.

Table 3
Phase change performance and thermal characteristics of MEPCMs with TiO_2-PUA shell with different size.

Stirring speed (rpm)	Capsule size (μm)	Crystallization		Melting		L_{TGA} (%)	E_{en} (%)	E_{es} (%)	C_{es} (%)
		T_c (°C)	ΔH_c (J/g)	T_m (°C)	ΔH_m (J/g)				
900	300	24.36	179.8 ± 0.04	29.66	181.1 ± 0.03	72.8	77.3	77.1	99.7
1200	200	23.96	147.8 ± 0.05	29.58	149.4 ± 0.10	65.2	63.5	63.4	99.9
1500	100	23.74	125.5 ± 0.01	29.44	127.0 ± 0.05	56.5	54.0	53.9	99.8

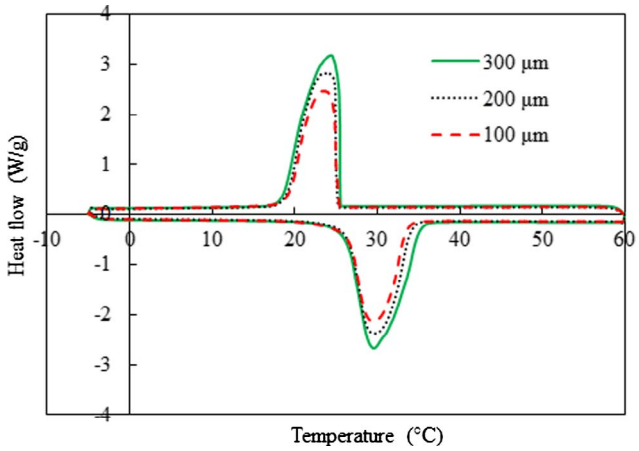

Fig. 9. DSC curves of MEPCMs with TiO_2-PUA shell with different size.

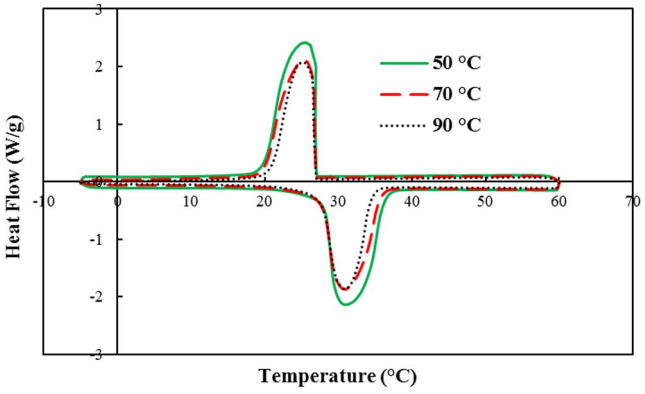

Fig. 10. DSC curves of MEPCMs with TiO_2-PUA shell synthesized at different reaction temperature.

4. Conclusion

This study presents a novel approach to synthesize MEPCMs with inorganic TiO_2 shell via a two-step liquid phase deposition (LPD) at low temperature. MEPCM pre-microcapsules with PUA shell were first synthesized through interfacial polymerization in oil-in-water emulsion, followed by LPD of TiO_2 on the surface of pre-microcapsules in solution. The thin PUA shell effectively stabilized and prevented coalescence of PCM micro-droplets and served as the hard template for deposition of TiO_2. The two-step synthesis approach results in high yield of microcapsules and the MEPCMs with composite TiO_2-PUA shell integrate advantages of both organic and inorganic shells.

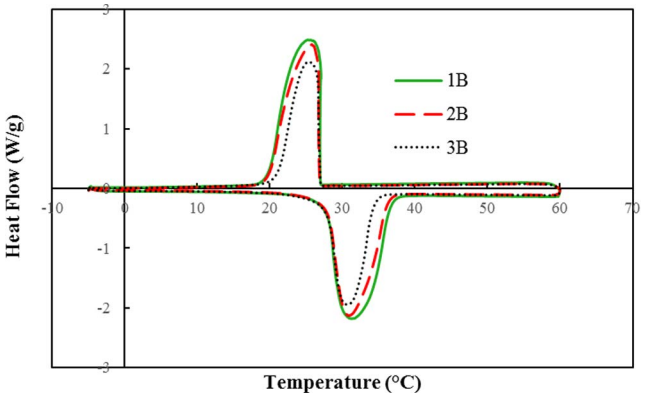

Fig. 11. DSC curves of MEPCMs with TiO_2-PUA shell fabricated with different H_3BO_3-to-$(NH_4)_2TiF_6$ ratio.

Influence of key synthesis parameters were studied and the resulting MEPCMs were characterized. The microcapsules had a well-defined core-shell structure with around 73 wt.% of core fraction and 10 μm thick dense composite TiO_2-PUA shell, which is thermally stable and durable and effectively lowers the evaporation and prevents leakage of the core material even under repeated heating and cooling. The MEPCMs showed mitigated supercooling and faster thermal response owing to the large surface area of microcapsules together with the high thermal conductivity of TiO_2. The thermal storage capacity of the MEPCMs can reach 99.9%, which indicates that core *n*-octadecane performs well and is able to fully exert its function during the melting and freezing cycle. TiO_2-PUA MEPCM-modified cement pastes showed distinct latent heat storage capacity. This suggests that the newly developed TiO_2-PUA MEPCMs have the potential to be incorporated into various matrix for imparting latent heat storage capability into building elements, energy systems, and textile. Further study is ongoing to impart photocatalysis function into the composite TiO_2-PUA shell.

Acknowledgement

The authors would like to acknowledge financial support from the Agency for Science, Technology and Research (A*STAR) – Ministry of National Development (MND), Singapore (SERC132 176 0014).

Table 4
Phase change performance and thermal characteristics of MEPCMs with TiO_2-PUA shell synthesized at different reaction temperature.

Temp (°C)	Crystallization		Melting		L_{TGA} (%)	E_{en} (%)	E_{es} (%)	C_{es} (%)
	T_c (°C)	ΔH_c (J/g)	T_m (°C)	ΔH_m (J/g)				
50	23.57	154.2 ± 0.10	29.65	155.7 ± 0.20	71.8	66.2	66.1	99.9
70	23.69	131.6 ± 0.10	29.48	134.2 ± 0.10	61.7	57.0	56.8	99.6
90	23.74	125.5 ± 0.01	29.44	127.0 ± 0.05	56.5	54.0	53.9	99.8

Table 5
Phase change performance and thermal characteristics of MEPCMs with TiO_2-PUA shell fabricated with different H_3BO_3-to-$(NH_4)_2TiF_6$ ratio.

H_3BO_3-to-$(NH_4)_2TiF_6$ ratio	Crystallization		Melting		L_{TGA} (%)	E_r (%)	E_{en} (%)	C_{es} (%)
	T_c (°C)	ΔH_c (J/g)	T_m (°C)	ΔH_m (J/g)				
1	23.14	163.3 ± 0.10	29.84	165.4 ± 0.10	74.3	70.3	70.1	99.7
2	23.71	142.9 ± 0.06	29.32	144.3 ± 0.10	66.2	61.3	61.3	99.9
3	23.74	125.5 ± 0.01	29.44	127.0 ± 0.05	56.5	54.0	53.9	99.8

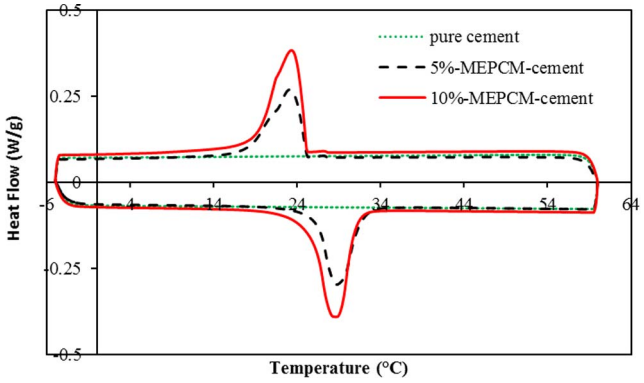

Fig. 12. DSC curves of TiO_2-PUA MEPCM-modified cement pastes.

References

[1] Nelson G. Microencapsulation in textile finishing. Rev Prog Coloration 2001;31:57–64.
[2] Cabeza LF, Castell A, Barreneche C, de Gracia A, Fernández AI. Materials used as PCM in thermal energy storage in buildings: a review. Renew Sustain Energy Rev 2011;15:1675–95.
[3] Jankowski NR, McCluskey FP. A review of phase change materials for vehicle component thermal buffering. Appl Energy 2014;113:1525–61.
[4] Ling ZY, Wang FX, Fang XM, Gao XN, Zhang ZG. A hybrid thermal management system for lithium ion batteries combining phase change materials with forced-air cooling. Appl Energy 2015;148:403–9.
[5] Jiang BB, Wang XD, Wu DZ. Fabrication of microencapsulated phase change materials with TiO_2/Fe_3O_4 hybrid shell as thermoregulatory enzyme carriers: a novel design of applied energy microsystem for bioapplications. Appl Energy 2017;201:20–33.
[6] Liu M, Saman W, Bruno F. Development of a novel refrigeration system for refrigerated trucks incorporating phase change material. Appl Energy 2012;92:336–42.
[7] Smith CJ, Forster PM, Crook R. Global analysis of photovoltaic energy output enhanced by phase change material cooling. Appl Energy 2014;126:21–8.
[8] Kosny J, Stovall TK, Shrestha SS, Yarbrough DW. Theoretical and experimental thermal performance analysis of complex thermal storage membrane containing bio-based phase change material (PCM). Oak Ridge National Laboratory (ORNL); Building Technologies Research and Integration Center; 2010.
[9] James B, Delaney P. Phase change materials: are they part of our energy efficient future? In: Proceedings of the 2012 ACEEE summer study on energy efficiency in buildings, California, USA; 2012. p. 3–160 to 3–72.
[10] Lei J, Yang J, Yang E-H. Energy performance of building envelopes integrated with phase change materials for cooling load reduction in tropical Singapore. Appl Energy 2016;162:207–17.
[11] Hawlader MN, Uddin MS, Khin MM. Microencapsulated PCM thermal energy storage system. Appl Energy 2003;74:195–202.
[12] Salunkhe PB, Shembekar PS. A review on effect of phase change material encapsulation on the thermal performance of a system. Renew Sustain Energy Rev 2012;16:5603–16.
[13] Memon SA. Phase change materials integrated in building walls: a state of the art review. Renew Sustain Energy Rev 2014;31:870–906.
[14] Leitch P, Tassinari T. Interactive textiles: new materials in the new millennium. J Ind Text 2000;29:173–90.
[15] Suryanarayana C, Rao K, Kumar D. Preparation and characterization of microcapsules containing linseed oil and its use in self–healing coatings. Prog Org Coat 2008;63:72–8.
[16] Chen Z, Cao L, Fang GY, Shan F. Synthesis and characterization of microencapsulated paraffin microcapsules as shape–stabilized thermal energy storage materials. Nanosc Microsc Therm 2013;17:112–23.
[17] Zhao CY, Zhang GH. Review on microencapsulated phase change materials (MEPCMs): fabrication, characterization and applications. Renew Sustain Energy Rev 2011;15:3813–32.
[18] Mondal S. Phase change materials for smart textiles – an overview. Appl Therm Eng 2008;28:1536–50.
[19] Ascione F, Bianco N, De Masi RF, de' Rossi F, Vanoli GP. Energy refurbishment of existing buildings through the use of phase change materials: energy savings and indoor comfort in the cooling season. Appl Energy 2014;113:990–1007.
[20] Lei JW, Kumarasamy K, Zingre KT, Yang JL, Wan MP, Yang EH. Cool colored coating and phase change materials as complementary cooling strategies for building cooling load reduction in tropics. Appl Energy 2017;190:57–63.
[21] Zhang HZ, Wang XD, Wu DZ. Silica encapsulation of n-octadecane via sol–gel process: a novel microencapsulated phase–change material with enhanced thermal conductivity and performance. J Colloid Interface Sci 2010;343:246–55.
[22] Li BX, Liu TX, Hu LY, Wang YF, Gao L. Fabrication and properties of microencapsulated paraffin@SiO_2 phase change composite for thermal energy storage. Sustain Chem Eng 2013;1:374–80.
[23] Zhang HZ, Sun SY, Wang XD, Wu DZ. Fabrication of microencapsulated phase change materials based on n-octadecane core and silica shell through interfacial polycondensation. Colloids Surf A Physicochem Eng Asp 2011;389:104–17.
[24] Wang LY, Tsai PS, Yang YM. Preparation of silica microspheres encapsulating phase–change material by sol–gel method in O/W emulsion. J Microencapsul 2006;23:3–14.
[25] Yu SY, Wang XD, Wu DZ. Microencapsulation of n-octadecane phase change material with calcium carbonate shell for enhancement of thermal conductivity and serving durability: synthesis, microstructure, and performance evaluation. Appl Energy 2014;114:632–43.
[26] Cahill DG, Allen TH. Thermal conductivity of sputtered and evaporated SiO_2 and TiO_2 optical coatings. Appl Phys Lett 1994;65:309–11.
[27] Touloukian YS. Thermophysical properties of matter. New York: IFI/Plenum; 1970.
[28] Cao L, Tang F, Fang GY. Preparation and characteristics of microencapsulated palmitic acid with TiO_2 shell as shape-stabilized thermal energy storage materials. Sol Energy Mater Solar Cell 2014;123:183–8.
[29] Chai LX, Wang XD, Wu DZ. Development of bifunctional microencapsulated phase change materials with crystalline titanium dioxide shell for latent-heat storage and photocatalytic effectiveness. Appl Energy 2015;138:661–74.
[30] McClements DJ. Nanoemulsions versus microemulsions: terminology, differences, and similarities. Soft Matter 2012;8:1719–29.
[31] Pereira da Cunha J, Eames P. Thermal energy storage for low and medium temperature applications using phase change materials – a review. Appl Energy 2016;177:227–38.
[32] Al-Shannaq R, Kurdi J, Al-Muhtaseb S, Farid M. Innovative method of metal coating of microcapsules containing phase change materials. Solar Energy 2016;129:54–64.
[33] Bellemare JV. Thermally reflective encapsulated phase change pigment. US Patent 2007; No. 0031652 A1.
[34] Zhang X, Fan Y, Tao X, Yick K. Fabrication and properties of microcapsules and nanocapsules containing n-octadecane. Mater Chem Phys 2004;88:300–7.
[35] Zhang H, Wang XD. Synthesis and properties of microencapsulated n-octadecane with polyurea shells containing different soft segments for heat energy storage and thermal regulation. Sol Energy Mater Solar Cell 2009;93:1366–76.
[36] Brown WE, Green AH, Cedel TE, Cairns J. Biochemistry of protein-isocyanate interactions: a comparison of the effects of aryl vs. Alkyl Isocyanates. J Environ Health Perspect 1987;72:5–11.
[37] Pearson R, Williams E. Interfacial polymerization of an isocyanate and a diol. J Polym Sci Polym Chem 1985;23:9–18.
[38] Sun DW, An JL, Wu G, Yang JL. Double-layered reactive microcapsules with excellent thermal and non-polar solvent resistance for self-healing coatings. J Mater Chem A 2015;3:4435–44.
[39] Ilium L. Chitosan and its use as a pharmaceutical excipient. Pharm. Res. 1998;15:1326–33.
[40] Deki S, Aoi Y, Asaoka Y, Kajinami A, Mizuhata M. Monitoring the growth of titanium oxide thin films by the liquid-phase deposition method with a quartz crystal microbalance. J Mater Chem 1997;7:733–6.
[41] Masuda Y, Sugiyama T, Seo WS, Koumoto K. Deposition mechanism of anatase TiO_2 on self-assembled monolayers from an aqueous solution. Chem Mater 2003;15:2469–75.
[42] Wamser C. Equilibria in the system boron trifluoride-water. J Am Chem Soc 1951;73:409–16.
[43] Connor PA, Dobson KD, McQuillan AJ. Infrared spectroscopy of the TiO_2/aqueous solution interface. Langmuir 1999;15:2402–8.
[44] Vasconcelos DC, Costa VC, Nunes EH, Sabioni AC, Gasparon M, Vasconcelos WL. Infrared spectroscopy of titania sol-gel coatings on 316L stainless steel. Mater Sci Appl 2011;2:1375–82.
[45] Zimbone M, Cacciato G, Buccheri MA, Sanz R, Piluso N, Reitano R. Photocatalytical activity of amorphous hydrogenated TiO_2 obtained by pulsed laser ablation in liquid. Mat Sci Semiconduct Proc 2016;40:28.
[46] Yilgor E, Yurtsever E, Yilgor I. Hydrogen bonding and polyurethane morphology. II. Spectroscopic, thermal and crystallization behavior of polyether blends with 1,3-

dimethylurea and a model urethane compound. Polymer 2002;43:6561–8.
[47] Mattia J, Painter P. A comparison of hydrogen bonding and order in a polyurethane and poly(urethane-urea) and their blends with poly (ethylene glycol). Macromolecules 2007;40:1546–54.
[48] Sanchez-Ferrer A, Rogez D, Martinoty P. Synthesis and characterization of new PUA elastomers by sol/gel chemistry. Macromol Chem Phys 2010;211:1712–21.
[49] Tatiya PD, Hedaoo RK, Mahulikar PP, Gite VV. Novel polyurea microcapsules using dendritic functional monomer: synthesis, characterization, and its use in self-healing and anticorrosive polyurethane coatings. Ind Eng Chem Res 2013;52:1562–70.
[50] Wu G, An JL, Sun DW, Tang XZ, Xiang Y, Yang JL. Robust microcapsules with polyurea/silica hybrid shell for one-part self-healing anticorrosion coatings. J Mater Chem A 2014;2:11614–20.
[51] Su YL, Liu GM, Xie BQ, Fu DS, Wang DJ. Crystallization features of normal alkanes in confined geometry. Acc Chem Res 2014;47:192–201.
[52] Jiang K, Su YL, Xie BQ, Jiang SC, Zhao Y, Wang DJ. Effect of geometrical confinement on the nucleation and crystallization behavior of n-alkane mixtures. J Phys Chem B 2008;112:16485–9.
[53] Tcholakova S, Denkov ND, Danner T. Role of surfactant type and concentration for the mean drop size during emulsification in turbulent flow. Langmuir 2004;20:7444–58.
[54] Djakovic L, Dokic P, Radivojevic P, Sefer I, Sovilj V. Action of emulsifiers during homogenization of o/w emulsions. Colloid Polym Sci. 1987;265:993–1000.